Evaluation of Collateral Source Characteristics With 3-Dimensional Analysis Using Micro–X-Ray Computed Tomography

Yuichiro Arima, MD, PhD; Seiji Hokimoto, MD, PhD; Noriaki Tabata, MD; Osamu Nakagawa, MD, PhD; Asahi Oshima; Yosuke Matsumoto; Takahiro Sato, ME; Toshifumi Mukunoki, Dr.(Eng); Jun Otani, PhD; Masanobu Ishii, MD; Michie Uchikawa, BS; Eiichiro Yamamoto, MD, PhD; Yasuhiro Izumiya, MD, PhD; Koichi Kaikita, MD, PhD; Hisao Ogawa, MD, PhD; Koichi Nishiyama, MD, PhD; Kenichi Tsujita, MD, PhD

Background—Collateral arteries provide an alternative blood supply and protect tissues from ischemic damage in patients with peripheral artery disease. However, the mechanism of collateral artery development is difficult to validate.

Methods and Results—Collateral arteries were visualized using micro–x-ray computed tomography. Developmental characteristics were assessed using confocal microscopy. We conducted a single-center, retrospective, observational study and assessed the dilatation of collateral arteries on ischemic sides. We quantified the vascular volume in both ischemic and nonischemic legs. A prominent increase in vascular volume was observed in the ischemic leg using a murine hind-limb ischemia model. We also performed qualitative assessment and confirmed that the inferior gluteal artery functioned as a major collateral source. Serial analysis of murine hind-limb vessel development revealed that the inferior gluteal artery was a remnant of the ischial artery, which emerged as a representative vessel on the dorsal side during hind-limb organogenesis. We retrospectively analyzed consecutive patients who were admitted for the diagnosis or treatment of peripheral artery disease. The diameter of the inferior gluteal artery on the ischemic side showed significant dilatation compared with that on the nonischemic side.

Conclusions—Our findings indicate that an embryonic remnant artery can become a collateral source under ischemic conditions. Flow enhancement in the inferior gluteal artery might become a novel therapeutic approach for patients with peripheral artery disease. (*J Am Heart Assoc*. 2018;7:e007800. DOI: 10.1161/JAHA.117.007800.)

Key Words: collateral circulation • computed tomography • peripheral artery disease

In peripheral artery disease (PAD), insufficient blood supply to the lower limb triggers intermittent claudication, a type of exercise-induced pain, and restricts activity.[1] In patients with PAD, the extent of collateral artery development influences the severity of tissue damage. Poor collateral supply results in critical limb ischemia.[2,3] However, the underlying mechanisms of collateral artery development have not been investigated in detail.

Murine hind-limb ischemia is the standard model used to assess angiogenic and wound healing capacity after organ ischemia.[4] This model can also be used to assess arteriogenesis.[5] However, the development of collateral arteries is not fully understood. One reason is that collateral artery remodeling occurs in a location remote from the ischemic tissue. Therefore, conventional histological analysis is not suitable, making it difficult to predict which vessel will develop into a collateral artery.

Clinical Perspective

What Is New?

- We developed a convenient comparison method for the murine hind-limb ischemia model by using micro–x-ray computed tomography.
- From topological data, we found that the inferior gluteal artery was remodeled and functioned as a prominent collateral artery on the ischemic side.

What Are the Clinical Implications?

- Arteries in the dorsal side of the human leg, including inferior gluteal artery, might become a novel therapeutic target for collateral enhancement therapy.

Micro–x-ray computed tomography (CT) is a useful tool for assessing morphological changes in a nondestructive manner.[6] Several reports have attempted to apply micro–x-ray CT to the murine hind-limb ischemia model.[7,8] Although these studies quantified vascular remodeling, they did not focus on collateral artery development.

In this study, we developed a convenient quantitative method of murine vascular remodeling by using micro–x-ray CT. Furthermore, we identified the inferior gluteal artery as a prominent collateral source whose function is equivalent to that of the femoral artery from a developmental perspective. Reactive dilation of the inferior gluteal artery was also observed in humans. These findings highlight a novel approach to the treatment of PAD.

Methods

The data that support the findings of this study are available from the corresponding author on reasonable request.

Animals

Femoral artery ligation was performed in male C57BL/6J or BALB/c mice, aged 8 to 10 weeks. Jcl:ICR embryos were harvested for developmental analysis. We mated Jcl:ICR mice, aged 6 to 10 weeks. The embryonic ages were determined through timed mating, with the appearance of a vaginal plug considered embryonic day 0.5. All mice were housed in an environmentally controlled room at a temperature of 23±2°C and a relative humidity of 50% to 60% under a 12-hour light/12-hour dark cycle.

All procedures were performed in accordance with the Kumamoto University animal care guidelines (approval reference no. A28-047), which conform to the US National Institutes of Health *Guide for the Care and Use of Laboratory Animals* (publication no. 85-23, revised 1996).

Ligation of the Femoral Artery

The surgical procedures have been described previously.[5,9] Mice underwent the procedure at the age of 8 to 10 weeks. Inhalation anesthesia with isoflurane was performed, and the left femoral artery was selectively ligated just distal to the branching point of the proximal caudal femoral artery.[5] To ensure that the mice developed ischemia, we made 2 knots and cut the thread between them to prevent the formation of bridging collaterals in the ligated femoral artery.

Laser Doppler Perfusion Imaging

Mice were placed on a heating plate set at 37°C under inhalation anesthesia with isoflurane. A laser Doppler imager (Moor Instruments) was used to measure blood flow. We measured thenar blood flow in both limbs. Laser Doppler perfusion imaging was performed at baseline, immediately after surgery, and at 3, 7, 14, and 28 days after surgery.

Functional Scoring

Functional scoring was performed at 4 weeks after surgery. We used a mouse limb ischemia grading scale, as follows: 0 indicates autoamputation of greater than half lower limb; 1, gangrenous tissue of greater than half foot; 2, gangrenous tissue of less than half foot, with lower limb muscle necrosis; 3, gangrenous tissue of less than half foot, without lower limb muscle necrosis; 4, pale foot or gait abnormalities; and 5, normal). We used a modified mouse ischemia grading scale to detect less severe levels of ischemia, as follows: 0 indicates autoamputation of leg; 1, leg necrosis; 2, foot necrosis; 3, ≥2 toe discolorations; 4, 1 toe discoloration; 5, ≥2 nail discolorations; 6, 1 nail discoloration; and 7, no necrosis.[8,10]

Contrast Medium Injection

We performed contrast injections using a method described by Weyers et al.[11] At 30 minutes before the procedure, heparin, 1 U/g, was IP administered. Under deep inhalation anesthesia with isoflurane, the mice were decapitated and a 22-G catheter was introduced into the descending aorta. A warmed vasodilating solution (papaverine hydrochloride, 4 g/L; adenosine, 1 g/L; heparin, 1 U/mL) was perfused for 3 minutes at a fixed pressure between 13 and 15 kPa, and 4% paraformaldehyde in Phosphate Buffered Salts (PBS) was perfused for another 3 minutes. Contrast medium (Microfil) was prepared just before administration, and 2 mL of contrast medium was injected at a fixed pressure. The injected mice were incubated overnight at 4°C. The skin was removed and stored after further fixation in 10% formaldehyde solution.

X-Ray CT Scan

We used a microfocused x-ray CT scanner (TOSHIBA TOSCAN-NER 32300 FPD) installed at the X-Earth Center of Kumamoto University in 2010. This scanner obtains 360° radioscopic image data with an x-ray image intensifier by turning the table while irradiating the object with x-rays, which allows for the inspection of an object placed on a sample table. The radioscopic image data are then used in reconstruction calculations, which result in cross-sectional images. Because the polychromatic x-ray beam generated has a wide range of frequencies, corrections are made for the beam-hardening effect.

A flat panel detector enables 3-dimensional scanning with a cone-shaped x-ray beam. The scan speed depends on scanning conditions. The sample was placed on the table and scanned with a cone-shaped x-ray beam. During scanning, the table was rotated to obtain a 360° scan. A back-projection of x-ray attenuation was detected on the flat panel detector. The x-ray CT images obtained were free from the ring artifact normally seen because the scanner applied a filter function during the image reconstruction process. An x-ray tube voltage of 50 kV and a current of 600 μA were chosen, and the focus-to-center distance was defined as 75.2 mm. Therefore, the dimension of 1 voxel was $28.7 \times 28.7 \times 28.7$ μm in this study.

Data Processing

We used Fiji for data processing.[12] The threshold of vascular volume was defined as a value higher than muscular voxel values and lower than bone voxel values. To measure each voxel value, we used the right (nonligated) gastrocnemius as the reference for muscle and the femur as the reference for bone. For geometric analysis, we used ScanIP (Simpleware, Ltd) and calculated the diameter of arteries by using the cross-sectional area function.

Immunohistochemistry

Samples were fixed using 4% paraformaldehyde at 4°C overnight. Embryo cryosections (10 μm thick) were immunostained using the following probes: Griffonia Simplicifolia Lectin I (GSL I) isolectin B4, fluorescein isothiocyanate conjugate (Vector Laboratories FL-1201, 1:200), anti-actin, α-smooth muscle, Cy3 conjugate (SIGMA C6198, 1:500), and 4′6-diamidino-2-phenylindole (Dojindo 340-07971, 1:500). Section images were obtained using BZ-X710 (Keyence).

Whole Immunohistochemistry

Samples were fixed using 4% paraformaldehyde at 4°C. Small pieces were immersed in a blocking reagent (2% bovine serum albumin, 0.1% Triton X in PBS[+]) for several hours at 4°C.

Isolectin GS-IB4 (Thermo Fisher I32450, 1:500) and 4′6-diamidino-2-phenylindole (Dojindo 340-07971, 1:500) in the blocking reagent were incubated with the samples at 4°C for 48 hours.

Stained samples were fixed in 2% low-gelling agar, and CUBIC1 was used for tissue clearing.[13] Fluorescent signals were visualized with a computer-assisted confocal microscope (Leica DMi8). Obtained stacked images were reconstructed using Imaris (BITPLANE).

Ink Injection

The process of ink injection has been described previously.[14] Embryos were collected at appropriate stages and dipped into heparinized PBS. Then, ink (Kiwa-Guro, Sailor, Japan) was gently injected into the umbilical vessels or hearts with a glass micropipette. Samples were fixed in 4% paraformaldehyde solution.

Patient Analysis

This study retrospectively enrolled and analyzed 101 consecutive patients who were admitted to Kumamoto University Hospital between January 1, 2013 and March 31, 2017 for the diagnosis or treatment of PAD. We excluded patients undergoing hemodialysis and those lacking imaging data. We analyzed 28 patients with ipsilateral lesions at the femoral or iliac artery. The study flow chart is shown in Figure 1, and patient background is shown in the Table. We measured the diameter of the arteries using cross-sectional CT or magnetic resonance angiography.

All procedures were conducted in accordance with the Declaration of Helsinki and its amendments. The study protocol was approved by the human ethics committee of Kumamoto University (approval no. 1421). The informed consent requirement was waived because of the low risk of this study; also, we were unable to obtain direct consent from all subjects. Instead, we extensively announced the study protocol in the Kumamoto University Hospital and on our website (http://www.kumadai-junnai.com) and gave the opportunity for patients to withdraw from the study.

Statistical Analysis

Data of normally distributed continuous variables are expressed as mean±95% confidence interval. Two-group comparisons were analyzed by the Welch's t test. The data of laser Doppler perfusion imaging were analyzed by 2-way ANOVA with repeated measures, followed by multiple comparisons with the Bonferroni method. The data of diameter of the deep femoral arteries and inferior gluteal arteries were analyzed by paired t test. A 2-tailed $P < 0.05$ denoted the presence of a statistically significant difference. Statistical analyses were performed using Prism 7 (GraphPad Software Inc).
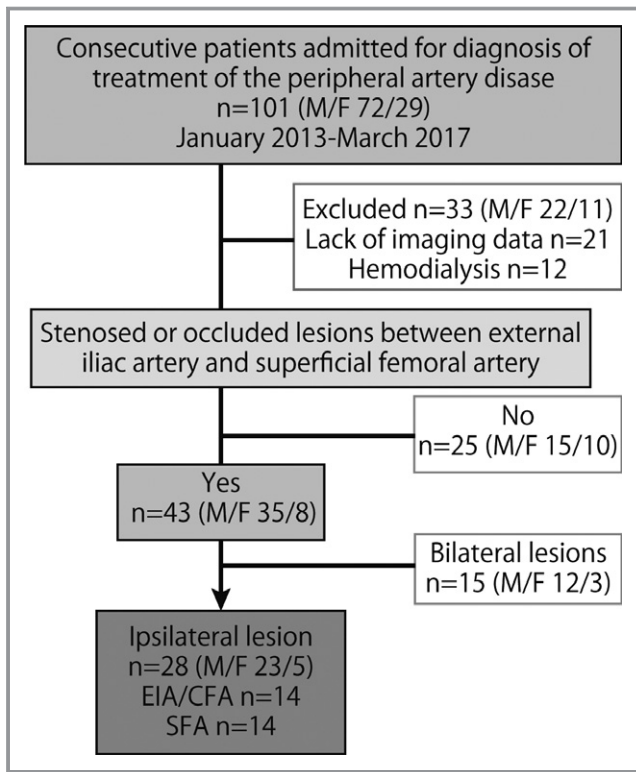
Figure 1. Flow chart. CFA indicates common femoral artery; EIA, external iliac artery; F, female; M, male; SFA, superficial femoral artery.

Results

Ligation of the Mid–Femoral Artery Generates Mild Hind-Limb Ischemia

In this study, we ligated the femoral artery just distal to its origin at the external iliac artery, where the proximal caudal femoral artery branches. We made 2 knots and cut the thread between them to ensure ischemia and to prevent the bridging by collateral vessels. The laser Doppler image showed an abrupt reduction in ipsilateral foot blood flow and a partial restoration at 1 month (Figure 2A and 2B). Functional scoring did not show any tissue damage in B6 mice (n=11) (Figure 2C and 2D). BALB/c mice showed slight tissue damage in the foot region, but severe ischemia in the calf could not be detected (ischemia score: left, ischemic side, 2.8±0.49; nonischemic side, 4.8±0.2; $P<0.01$ [Welch's t test]; modified ischemia score: left, ischemic side, 5.4±0.54; nonischemic side, 6.9±0.1; $P<0.05$ [Welch's t test]). Three-dimensional reconstruction of the micro–x-ray CT images did not show any destructive changes in the femur and tibia (Figure 2E and 2F). The long-axis diameter of each bone did not exhibit any significant differences between the ischemic and nonischemic sides (femur: ischemic side, 14.8±0.21 mm; nonischemic side, 14.9±0.17 mm; $P=0.560$ [Welch's t test]; tibia: ischemic

Table. Patient Characteristics

Baseline Characteristics	Values (n=28)
Age, y	70.4±8.2
Male sex, n (%)	23 (82.1)
Body mass index, kg/m^2	23.2±3.0
Hypertension, n (%)	26 (92.9)
Dyslipidemia, n (%)	21 (75.0)
Diabetes mellitus, n (%)	15 (53.6)
eGFR, mL/min	49.8±19.4
Stroke, n (%)	3 (10.7)
Current smoking, n (%)	10 (35.7)
History of heart failure, n (%)	4 (14.3)
History of PCI, n (%)	10 (35.7)
EF, %	60.9±8.2
LVDd, mm	43.3±5.2
IVSTd, mm	11.2±1.4
E/e'	13.3±3.3
Hemoglobin, g/dL	12.7±1.6
Hematocrit, %	38.2±4.2
Platelet count, 10^3/μL	207.9±69.6
Total protein, g/dL	6.8±0.4
Albumin, g/dL	3.8±0.3
TC, mg/dL	174.2±42.1
Triglyceride, mg/dL	140.1±76.0
LDL-C, mg/dL	108.2±33.1
HDL-C, mg/dL	47.2±10.8
ABI findings	
Control side	0.89±0.14
Ischemic side	0.66±0.24
Medications, n (%)	
β Blocker	7 (25.0)
CCB	6 (21.4)
ACEi	18 (64.3)
ARB	5 (17.9)
Aspirin	10 (35.7)

Data are mean±SD unless otherwise indicated. Data of these parameters were measured at the point of admission. ABI indicates ankle-brachial index; ACEi, angiotensin-converting enzyme inhibitor; ARB, angiotensin receptor blocker; CCB, calcium channel blocker; E/e', the ratio of mitral peak velocity of early filling (E) to early diastolic mitral annular velocity (e'); EF, left ventricular ejection fraction; eGFR, estimated glomerular filtration rate; HDL-C, high-density lipoprotein cholesterol; IVSTd, interventricular septum end-diastolic thickness; LDL-C, low-density lipoprotein cholesterol; LVDd, left ventricular end-diastolic dimension; PCI, percutaneous coronary intervention; and TC, total cholesterol.

side, 17.9±0.28 mm; nonischemic side, 17.8±0.04 mm; $P=0.794$ [Welch's t test]; n=4). From these data, our model was assumed to produce definite, but mild, hind-limb ischemia.
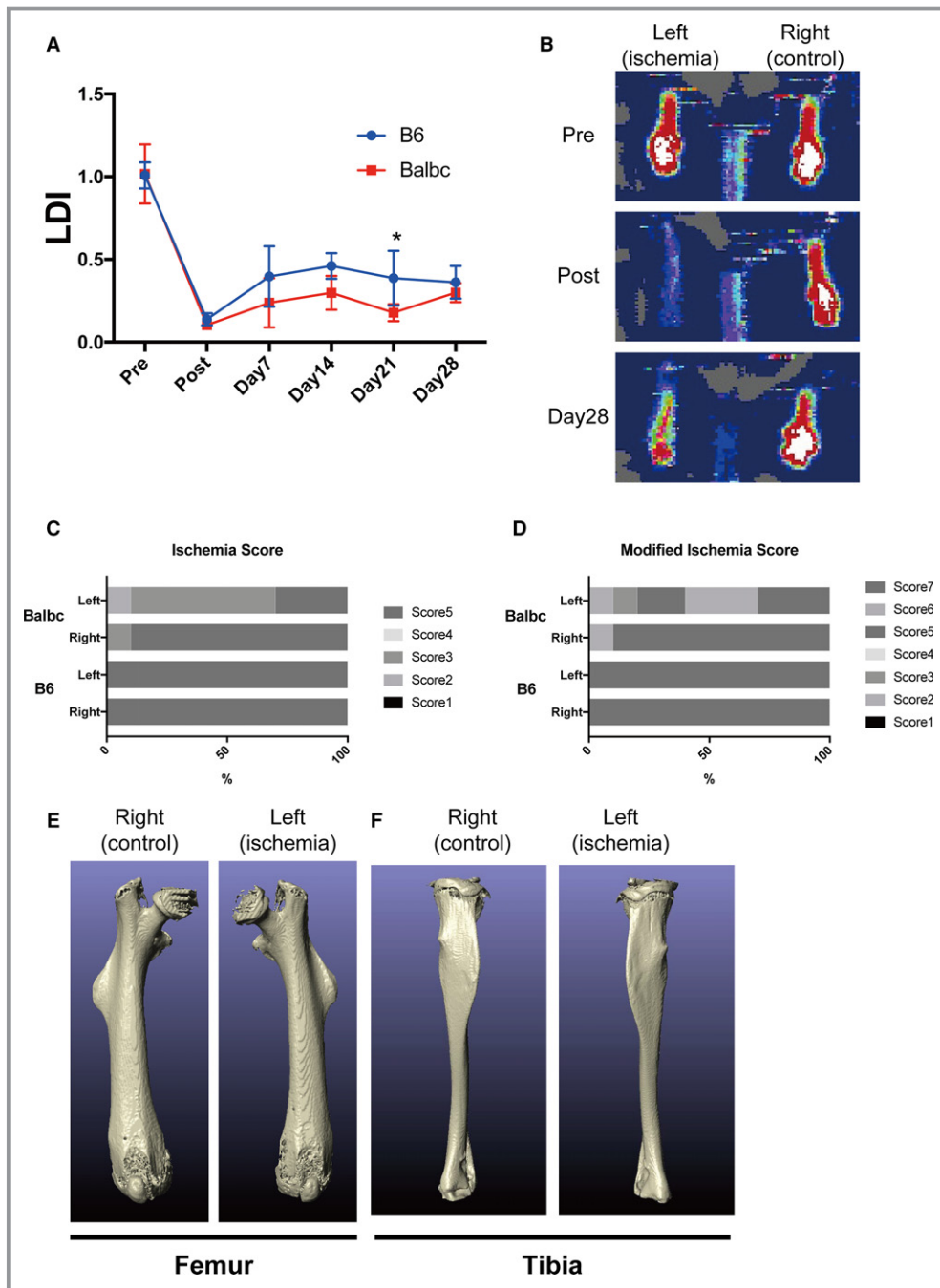
Figure 2. Murine hind-limb ischemia model. A, Serial changes in foot laser Doppler perfusion imaging (B6: n=11; BALB/c: n=10). The nonligated right side laser Doppler image (LDI) was divided by the ligated left side LDI. Two-way ANOVA showed significant differences between B6 and BALB/c mice (*P*<0.01), and Bonferroni's multiple comparisons test revealed significant differences at day 21 Data are mean±95% confidence interval. B, Representative images of foot blood flow. C, Ischemic score. We assessed BALB/c mice (n=10) and B6 mice (n=11) 4 weeks after the procedure. D, Modified ischemic score. We measured BALB/c mice (n=10) and B6 mice (n=11) 4 weeks after the procedure. E, Representative image of 3-dimensional reconstructed femur. F, Representative image of 3-dimensional reconstructed tibia. *P<0.05. Pre indicates Pre-Procedure; Post, Post-Procedure.
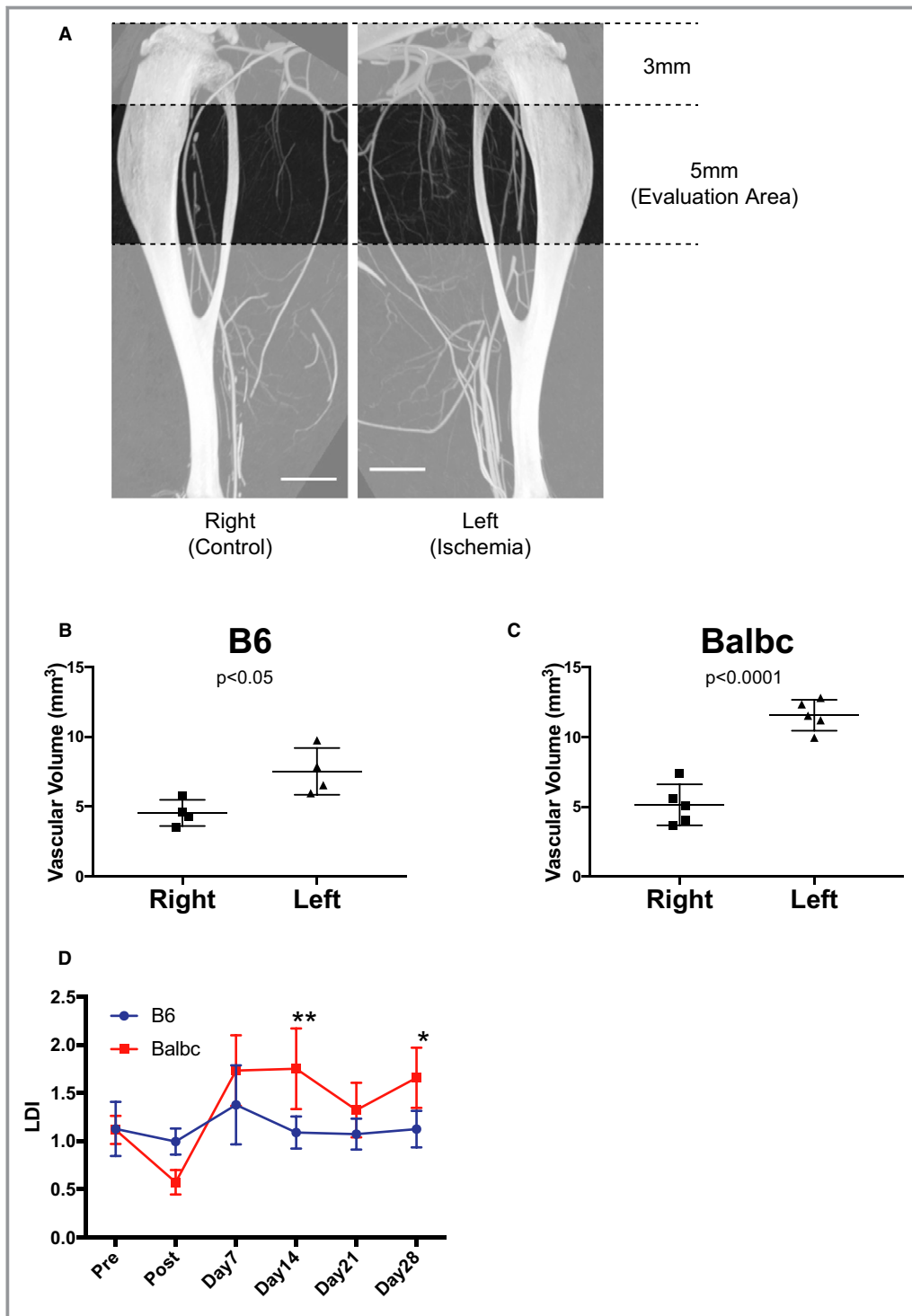
Figure 3. Quantitative assessment of vascular volume. A, Regions evaluated for quantitative analysis. The corresponding 5-mm regions of both sides are compared. B, Vascular volume differences in B6 mice (n=4). Left: ischemic side, 7.5 ± 0.84 mm^3; right: nonischemic side, 4.6 ± 0.47 mm^3 ($P<0.05$ [Welch's t test]). C, Vascular volume differences in BALB/c mice (n=4). Left: ischemic side, 11.6 ± 0.49 mm^3; right: nonischemic side, 5.2 ± 0.66 mm^3 ($P<0.0001$ [Welch's t test]). D, Serial changes in calf laser Doppler perfusion imaging (B6: n=11; BALB/c: n=10). The nonligated right side laser Doppler image (LDI) was divided by the ligated left side LDI. Two-way ANOVA showed significant differences between B6 and BALB/c mice ($P<0.01$); Bonferroni's multiple comparisons test revealed significant differences at day 14 and day 21. Data are shown as mean$\pm$95% confidence interval. *$P<0.05$, **$P<0.01$. Pre indicates Pre-Procedure; Post, Post-Procedure.
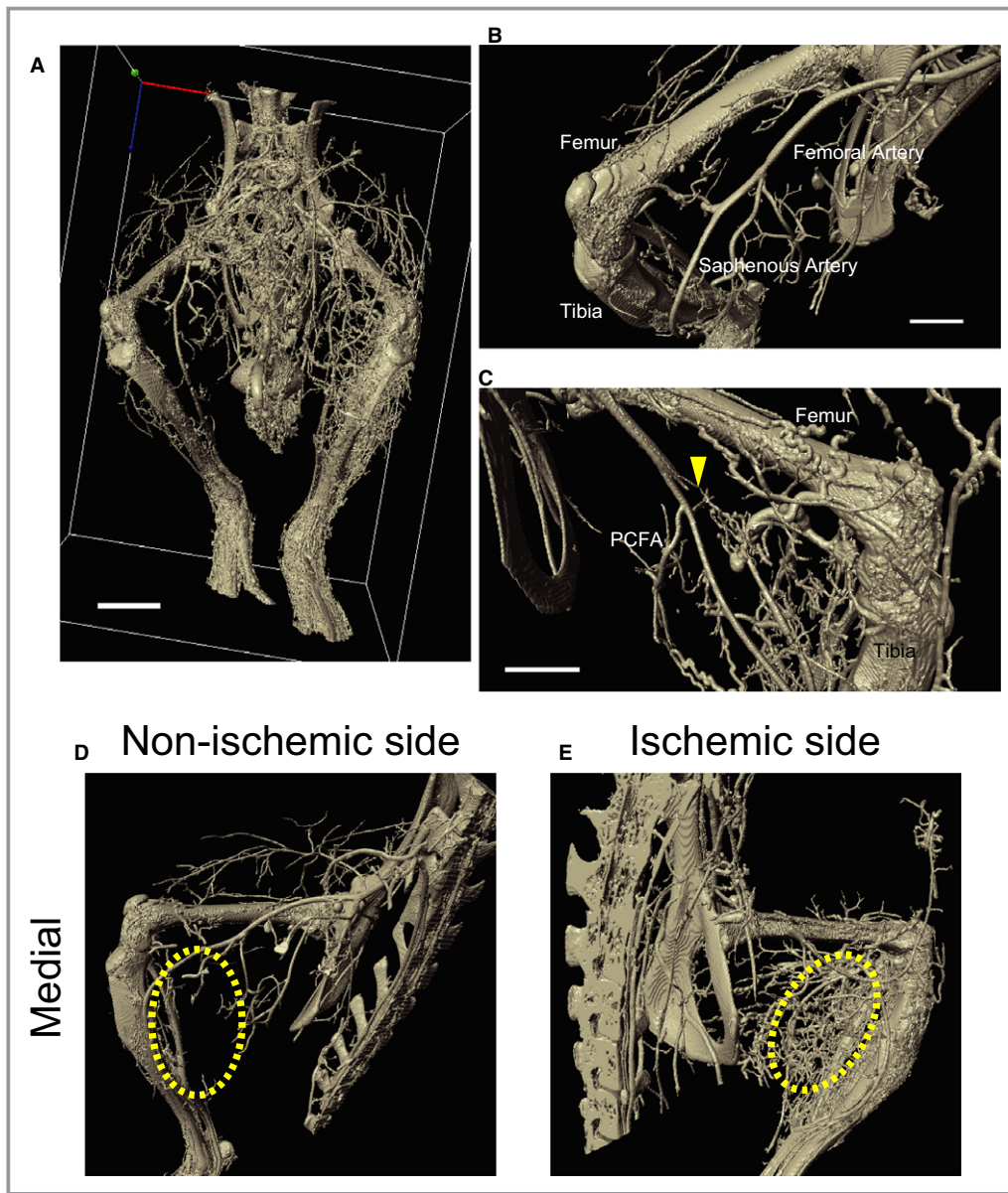
Figure 4. Three-dimensional reconstruction of the murine hind-limb image. A, Whole architecture of the lower body. The upper body and tail have been removed (bar=4 mm). B and C, Magnified image of the ligated region. Compared with the right, nonischemic side (B), the mid–femoral artery was cut on the left, ischemic side (arrowhead, C) (bar=2 mm). D and E, Remodeled arteries in the calf region. The calf regions are indicated by dashed yellow circles. PCFA indicates proximal caudal femoral artery.

Quantitative Assessment of Vascular Volume

We euthanized the mice at 1 month, and the arteries in the lower limb were filled with radiopaque dye. These mice were then imaged using micro–x-ray CT. The images were processed, and the vascular density area was extracted. We quantified vessel volume within 5 mm of the long axis of the tibia (Figure 3A). Both the B6 and BALB/c mice exhibited a significant increase in vascular volume on the ischemic side (B6: ischemic side, 7.5 ± 0.84 mm^3; nonischemic side, 4.6 ± 0.47 mm^3; n=4; $P<0.05$ [Welch's t test]; BALB/c: ischemic side, 11.6 ± 0.49 mm^3; nonischemic side, 5.2 ± 0.66 mm^3; n=5; $P<0.0001$ [Welch's t test]) (Figure 3B and 3C). It is known that postischemic recovery is different among strains and that BALB/c mice show poorer outcomes than C57BL/6 mice. The laser Doppler image in the foot showed similar findings in our study (Figure 2A). We also assessed serial calf flow (B6: n=11; BALB/c: n=10). Calf laser Doppler image showed a
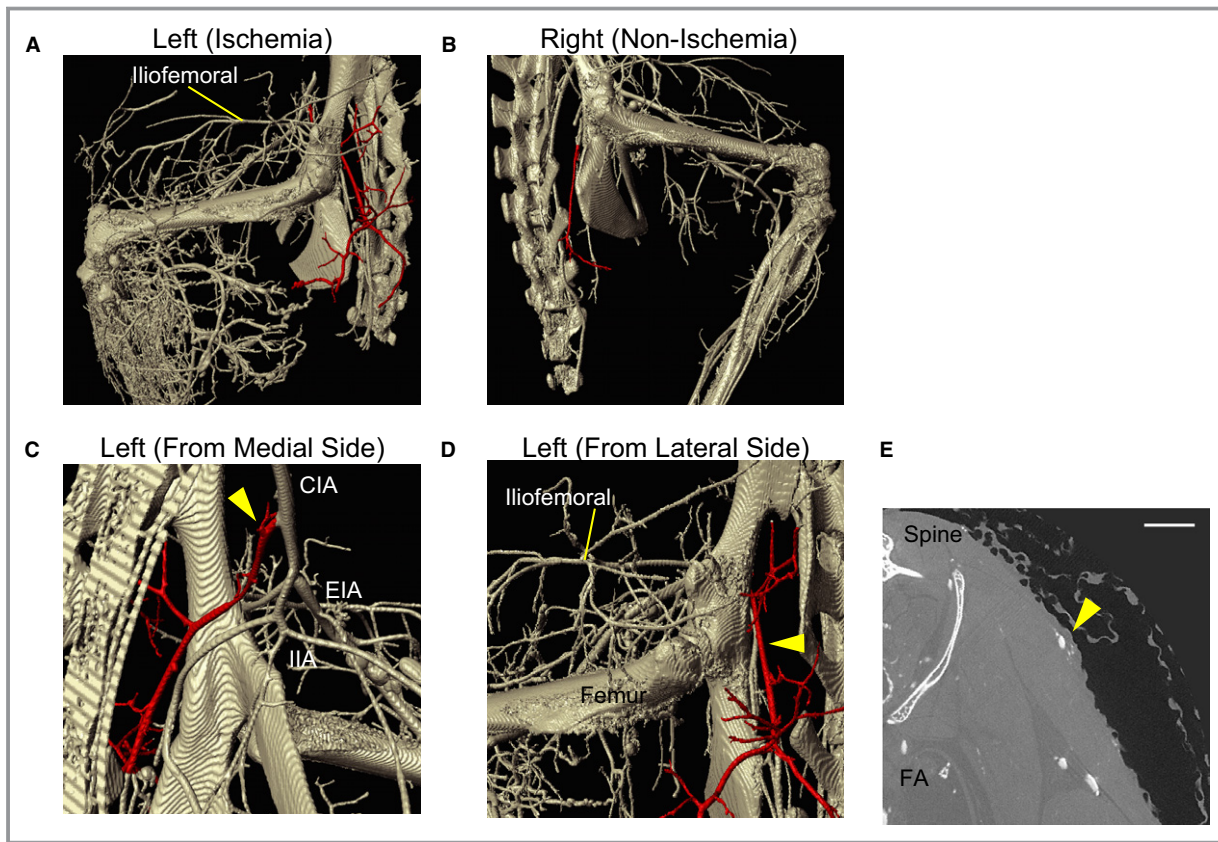
Figure 5. Anatomical characteristics of the inferior gluteal artery. A and B, Lateral side views of the left (A) and right (B) gluteal regions. The inferior gluteal artery is shown in red. C and D, Magnified images of the inferior gluteal artery (yellow arrowhead, red artery) from medial (C) and lateral (D) sides. The iliofemoral artery is also shown in Figure 4D. E, The inferior gluteal artery in a 2-dimensional computed tomography image (yellow arrowhead). F, Comparison of the cross-sectional areas of the inferior gluteal artery in B6 mice (n=4) (left: ischemic side, 0.026 ± 0.0010 mm^2; right: nonischemic side, 0.014 ± 0.0011 mm^2; n=4; $P<0.001$ [Welch's *t* test]). G, Comparison of the cross-sectional areas of the inferior gluteal artery in BALB/c mice (n=4) (left: ischemic side, 0.030 ± 0.0020 mm^2; right: nonischemic side, 0.020 ± 0.0015 mm^2; n=4; $P<0.05$ [Welch's *t* test]). H, Comparison of the cross-sectional areas of the inferior gluteal artery in B6 mice (n=4) (left: ischemic side, 0.030 ± 0.0012 mm^2; right: nonischemic side, 0.025 ± 0.0024 mm^2; n=4; $P=0.139$ [Welch's *t* test]). I, Comparison of the cross-sectional areas of the inferior gluteal artery in BALB/c mice (n=4) (left: ischemic side, 0.029 ± 0.0019 mm^2; right: nonischemic side, 0.027 ± 0.0016 mm^2; n=4; $P=0.465$ [Welch's *t* test]). CIA indicates common iliac artery; EIA, external iliac artery; FA, femoral artery; IGA, inferior gluteal artery; and IIA, internal iliac artery.

paradoxically enhanced laser Doppler image ratio in BALB/c mice ($P<0.01$, 2-way ANOVA) (Figure 3D).

These data indicate that prolonged ischemia induced remodeling and enlargement of mid- to large-diameter vessels, which were detectable with micro–x-ray CT analysis. Furthermore, BALB/c mice showed paradoxical vascular remodeling in the calf region, despite poor distal perfusion. The enhancement of calf blood flow corresponded to increased vascular volume in the ischemic calf region. However, this increased vascular volume and flow did not salvage the distal foot. This finding is an example of nonfunctional collateral vessel development and suggests that collateral artery development and also connection to the microcirculation are important for tissue salvage.

Reconstructed 3-Dimensional Images Indicate the Geographical Characteristics of the Ischemic Region

To assess the development of collateral arteries, we reconstructed the stacked images obtained with micro–x-ray CT into their corresponding 3-dimensional architecture (Figure 4A, Video S1). We confirmed that the ligation was performed at the proper position just distal to the site of the branching of the proximal caudal femoral artery (Figure 4B and 4C, Video S2). The reconstructed images also indicated significant development of remodeled vessels in the calf region on the ischemic side (Figure 4D and 4E, Video S2).
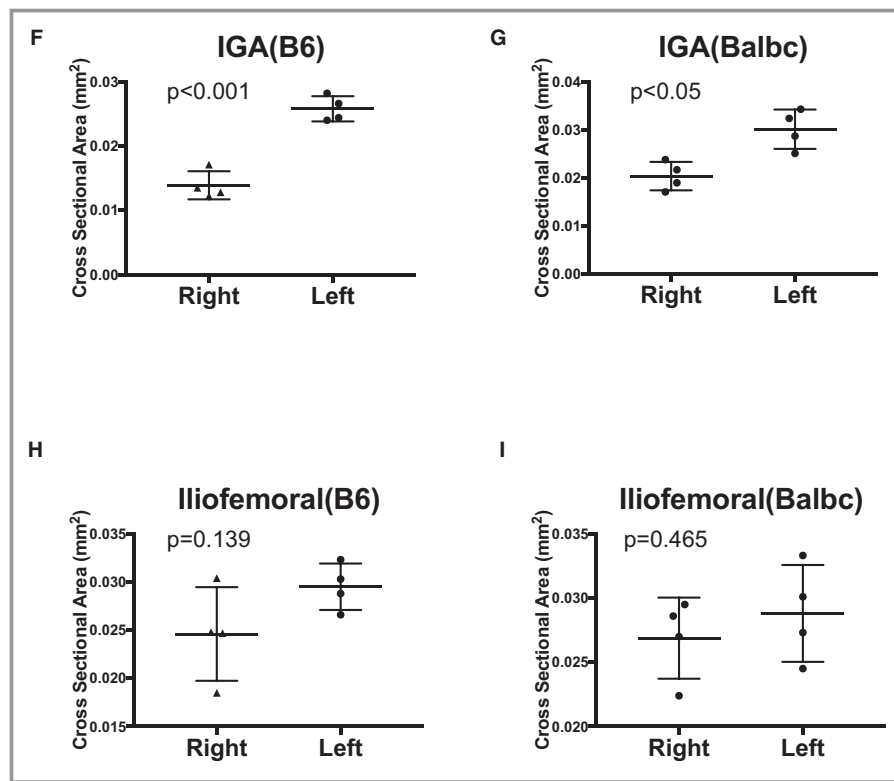
Figure 5. Continued

Inferior Gluteal Artery Functions as a Prominent Collateral Artery

We then focused on the source of collateral arteries. A prominent collateral artery was found on the lateral gluteal side (Figure 5A and 5B). This artery originated from the common iliac artery and traveled through the greater sciatic foramen (Figure 5C and 5D). It then branched and ran along the lateral surface of the gluteal and thigh regions (Figure 5E). From these anatomical characteristics, we identified this collateral as the inferior gluteal artery. The cross-sectional area of the inferior gluteal artery on the ischemic side was significantly dilated compared with that on the control side (B6: ischemic side, 0.026 ± 0.0010 mm^2; nonischemic side, 0.014 ± 0.0011 mm^2; n=4; $P<0.001$ [Welch's t test]; BALB/c: ischemic side, 0.030 ± 0.0020 mm^2; nonischemic side, 0.020 ± 0.0015 mm^2; n=4; $P<0.05$ [Welch's t test]) (Figure 5F and 5G). However, other prominent arteries did not show significant dilatation (iliofemoral artery, B6: ischemic side, 0.030 ± 0.0012 mm^2; nonischemic side, 0.025 ± 0.0024 mm^2; n=4; $P=0.139$ [Welch's t test]; BALB/c: ischemic side, 0.029 ± 0.0019 mm^2; nonischemic side, 0.027 ± 0.0016 mm^2; n=4; $P=0.465$ [Welch's t test]) (Figure 5H and 5I). From these data, the inferior gluteal artery functioned as the major collateral feeding artery.

Murine Inferior Gluteal Artery Is the Remnant of the Ischial Artery

In humans, the inferior gluteal artery is also known as the remnant of the proximal ischial artery.[15] A recent report showed that bone and vessel formation cooperatively proceed at the same time.[16] However, detailed developmental characteristics of the murine inferior gluteal artery are unknown. Therefore, we assessed the serial changes in the ischial artery and the development of the inferior gluteal artery by using 2- or 3-dimensional optical techniques.

First, we assessed the lower-limb buds at embryonic day 11. Section images revealed that the axial artery was formed by coalescing mesenchymal cells (Figure 6A through 6C). At this stage, obvious vascular remodeling has not yet occurred. Three-dimensional reconstruction and orthogonal images revealed that capillaries were uniformly distributed and formed the reticular vascular plexus (Figure 6D and Video S3).

At embryonic day 13.5, avascular condensed mesenchyme appeared in each segment of the limb buds (Figure 6E through 6J). Whole-mount vascular imaging revealed a symmetrical axial artery split at the stylopod and zeugopod (Figure 6K and 6L, Videos S4 and S5).

At embryonic day 15.5, ink injection revealed that prominent remodeled vessels appeared on the dorsoventral
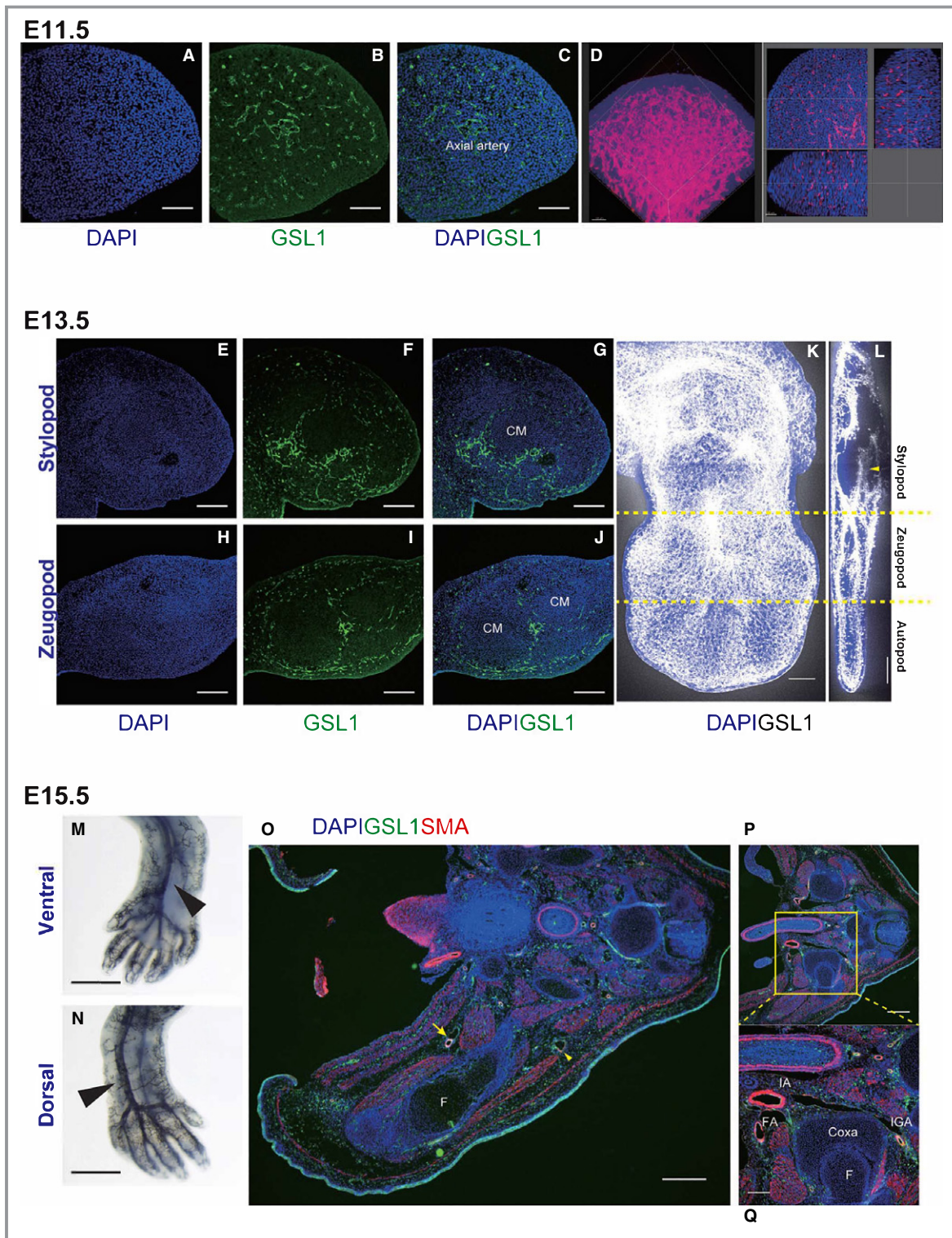
Figure 6. Vascular development in the lower limb. A through C, Section staining at embryonic day 11.5 (bar=100 μm). D, Whole-limb bud staining and orthogonal view at embryonic day 11.5 (bar=50 μm, see also Video S3). E through J, Section staining at embryonic day 13.5. K and L, Whole-limb bud staining at embryonic day 13.5 (K) and orthogonal view (L) (see also Videos S4 and S5). M and N, Remodeled arteries in the ventral (M) and dorsal (N) sides at embryonic day 15.5. A prominent artery was formed at the midline in each side (arrowheads). O, Section staining at embryonic day 15.5 (arrow, femoral artery [FA]; arrowhead, ischial artery). P and Q, Magnified image of the major sciatic space. The major sciatic space is indicated as a dashed circle. CM indicates condensed mesenchyme; Coxa, coxal bone; DAPI, 4′6-diamidino-2-phenylindole; F, femur; GSL1, Griffonia Simplicifolia Lectin I; IA, iliac artery; and IGA, inferior gluteal artery.

surfaces (Figure 6M and 6N). Section images also revealed that these prominent vessels developed simultaneously (Figure 6O) and corresponded to the ischial artery/vein and femoral artery/vein. The ischial artery crossed the major ischial space and communicated with the common iliac artery in the same manner as the inferior gluteal artery (Figure 6P and 6Q). From these data, the murine inferior gluteal artery was also considered as a remnant of the proximal part of the ischial artery.

Reactive Dilatation of the Inferior Gluteal Artery in Humans

Up to this point, we found the inferior gluteal artery to be dilated after femoral artery ligation in the murine model. Therefore, we assessed reactive dilatation of the inferior gluteal artery in humans with PAD. We retrospectively enrolled 101 patients and analyzed 28 who had ipsilateral stenosis or occlusion between the external iliac and superficial femoral arteries (Figure 1, Table). In the case of an occluded external iliac artery (Figure 7A), the inferior gluteal artery connected to the branches of the deep femoral artery

(Figure 7B and 7C). Then, the diameters of both arteries were compared. We did not detect significant changes in the diameters of the deep femoral arteries ($P=0.271$ [paired t test]) (Figure 7D); however, the inferior gluteal artery on the ischemic side was significantly dilated compared with that on the nonischemic side ($P<0.05$ [paired t test]) (Figure 7E). From these data, we discovered that the human inferior gluteal artery also functioned as a significant collateral artery.

Discussion

In this study, we developed a convenient comparison method for the murine hind-limb ischemia model by using micro–x-ray CT. From topological data, we found that the inferior gluteal artery was remodeled and functioned as a prominent collateral artery on the ischemic side. We also found that the architecture of the murine inferior gluteal artery was homologous to that of the ischial artery, which is a prominent dorsal vessel in mice. Furthermore, the inferior gluteal artery was also reactively dilated in humans with PAD.

Our findings demonstrate the conventional use of micro–x-ray CT for the assessment of collateral artery development. We
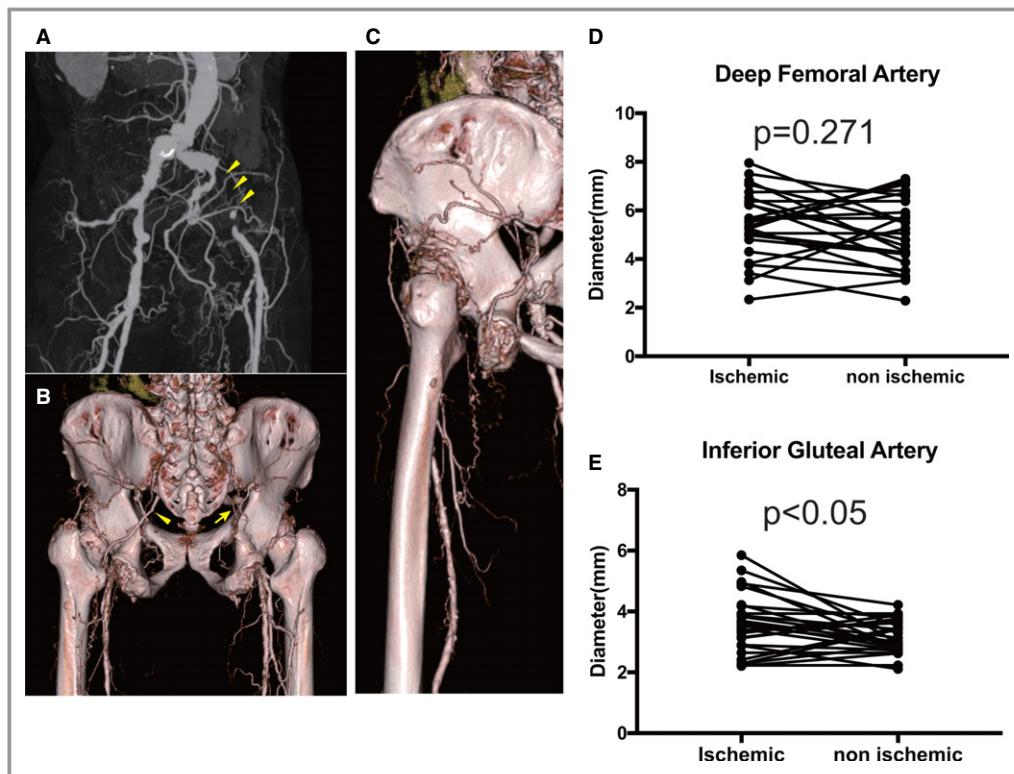

Figure 7. Reactive dilatation of the inferior gluteal artery in patients. A through C, Representative images of the inferior gluteal artery. The left external iliac artery was occluded (A, yellow arrowheads). The backside view shows the left inferior gluteal artery (yellow arrowhead) compared with that on the right side (yellow arrow) (B). C, The left inferior gluteal artery connects to the branches of the left deep femoral artery. D, Diameter of the deep femoral arteries (n=28). $P=0.271$ (paired t test was performed). E, Diameter of the inferior gluteal arteries (n=28). $P<0.05$ (paired t test was performed).
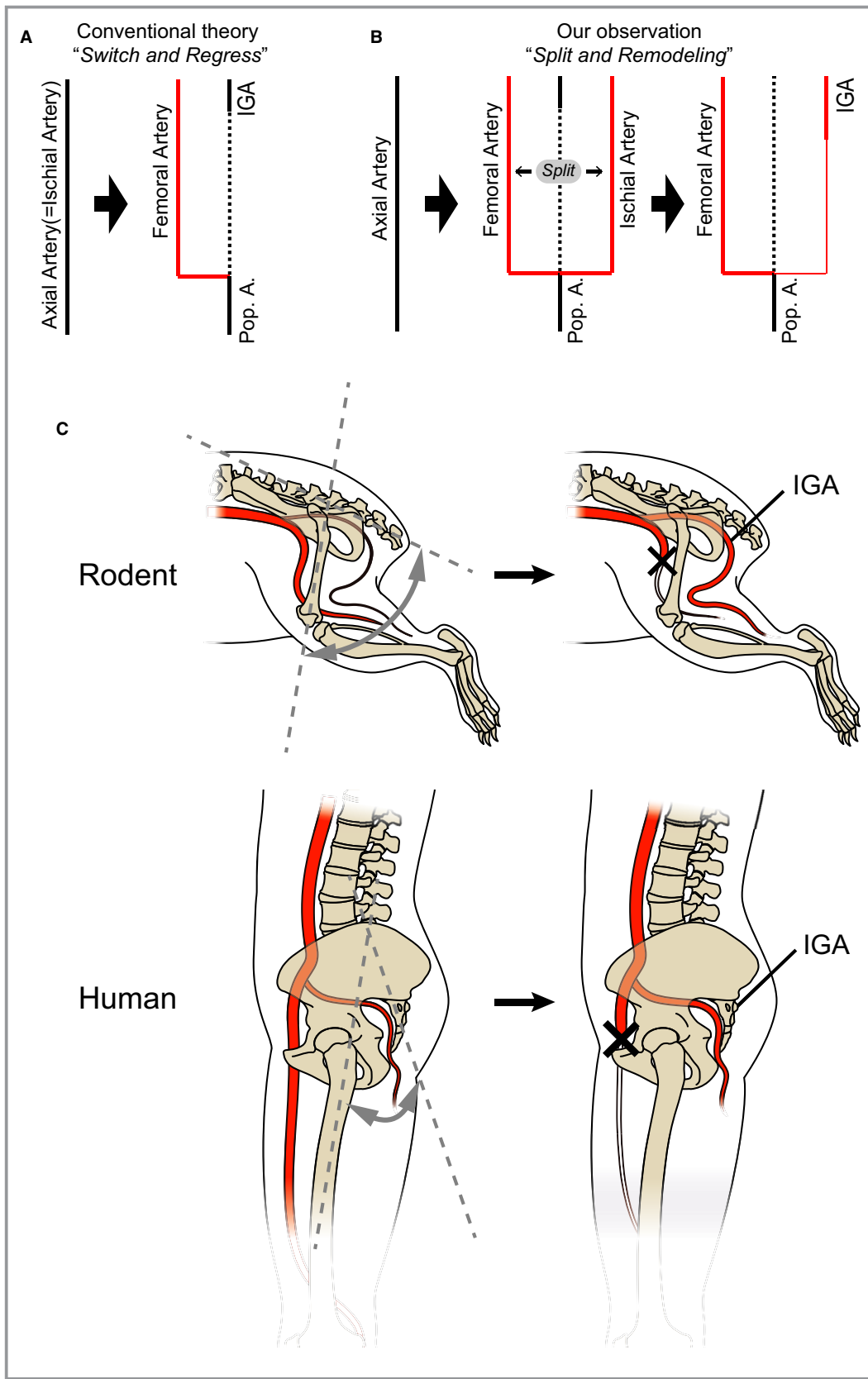
Figure 8. Summary illustrations. A, Conventional theory: "switch-and-regress" model. B, Our observation: "split-and-remodeling" model. C, Anatomical comparison between rodents and humans. IGA indicates inferior gluteal artery; and Pop. A., popliteal artery.

also identified the inferior gluteal artery as a useful site to assess when attempting to locate the collateral feeding artery. Furthermore, we also confirmed that reactive dilatation occurs in humans. These findings provide a novel therapeutic approach for collateral enhancement therapy. In animal experiments, microscopic observation restricts the evaluation fields and quantitative analysis is difficult in some cases. In this study, we developed a convenient evaluation method for the entire hind limb. By comparing the corresponding regions of both sides, the vascular volume can be easily quantified. Furthermore, micro–x–ray CT facilitates the analysis of remote parts. These advantages enable the analysis of collateral artery development.

In limb development, the axial artery is primarily generated and then switches to the femoral artery. Most of the axial artery disappears, and the proximal remnant portion is thought to be the inferior gluteal artery.[17] This "switch-and-regress" concept is considered the conventional theory (Figure 8A). However, our observation of murine hind-limb vessel development revealed that the femoral artery and the dorsal ischial artery developed at the same time. Their developmental pattern exhibited a mirror image to that of the ventral–dorsal axis. The axial artery was located at the center of the limb bud and seemed to have split into the femoral and ischial arteries. In rodents and humans, the femoral artery becomes the chief artery of the lower (hind) limb. However, the ischial artery is the chief artery of the hind limb in many vertebrates.[18] These ontogenetic and phylogenetic characteristics provide a new "split and remodeling" concept (Figure 8B).

Compared with the murine model, the development of the inferior gluteal artery in humans is not as extensive. In particular, it was difficult to detect sufficient collateral development in the thigh region. A previous report showed that the morphological changes of the hip joint restricted the remnant of the ischial artery.[19] We further hypothesized that bipedal walking and standing posture influence the development of collateral arteries. Bipedal walking is a human characteristic.[20] In a murine model, the inferior gluteal artery courses along the outermost lateral surface and travels to the calf region in an abbreviated manner. However, the standing posture of humans increases the distance from the gluteal region to the calf region. These changes might have evolutionarily limited the collateral growth of the inferior gluteal artery (Figure 8C).

Furthermore, a supine position is related to some diseases.[21] Gravity is involved in the pathogenesis of acute respiratory distress syndrome, and release from gravity has been tested in treatment.[22] The inferior gluteal arteries are dorsal arteries, and a supine position easily disturbs their flow. Therefore, posture may be involved in the insufficient growth of collaterals in humans.

Our study has several limitations. Our model is that of mild acute hind-limb ischemia. However, the pathogenesis of PAD proceeds chronically. We observed the same phenomena in both situations, but another model of chronic hind-limb ischemia will be required for further analysis. Angiogenesis and collateral artery development are regulated by humoral factors, mesenchymal stem cells, mechanical stress, and other factors.[23–25] We did not investigate their roles in our ischemic model, and further study will be required.

Many invisible arteries also developed in our experiments. This finding indicates that small collateral channels can be remodeled by specific stimuli. Through the identification of factors that enhance collateral artery development, a novel therapeutic approach may be developed for patients with PAD.

Acknowledgments

Sources of Funding

Disclosures

None.

References

1. Norgren L, Hiatt WR, Dormandy JA, Nehler MR, Harris KA, Fowkes FG, Group TIW, Bell K, Caporusso J, Durand-Zaleski I, Komori K, Lammer J, Liapis C, Novo S, Razavi M, Robbs J, Schaper N, Shigematsu H, Sapoval M, White C, White J, Clement D, Creager M, Jaff M, Mohler E III, Rutherford RB, Sheehan P, Sillesen H, Rosenfield K. Inter-society consensus for the management of peripheral arterial disease (TASC II). Eur J Vasc Endovasc Surg. 2007;33(suppl 1):S1–S75.

2. Dormandy JA, Rutherford RB; TASC Working Group. TransAtlantic Inter-Society Consensus (TASC). Management of peripheral arterial disease (PAD). J Vasc Surg. 2000;31:S1–S296.

3. Engelhardt M, Boos J, Bruijnen H, Wohlgemuth W, Willy C, Tannheimer M, Wolfle K. Critical limb ischaemia: initial treatment and predictors of amputation-free survival. Eur J Vasc Endovasc Surg. 2012;43:55–61.

4. Cao R, Brakenhielm E, Pawliuk R, Wariaro D, Post MJ, Wahlberg E, Leboulch P, Cao Y. Angiogenic synergism, vascular stability and improvement of hind-limb ischemia by a combination of PDGF-BB and FGF-2. Nat Med. 2003;9:604–613.

5. Limbourg A, Korff T, Napp LC, Schaper W, Drexler H, Limbourg FP. Evaluation of postnatal arteriogenesis and angiogenesis in a mouse model of hind-limb ischemia. Nat Protoc. 2009;4:1737–1746.

6. Zagorchev L, Oses P, Zhuang ZW, Moodie K, Mulligan-Kehoe MJ, Simons M, Couffinhal T. Micro computed tomography for vascular exploration. J Angiogenes Res. 2010;2:7.

7. Zhuang ZW, Gao L, Murakami M, Pearlman JD, Sackett TJ, Simons M, de Muinck ED. Arteriogenesis: noninvasive quantification with multi-detector row CT angiography and three-dimensional volume rendering in rodents. Radiology. 2006;240:698–707.

8. Westvik TS, Fitzgerald TN, Muto A, Maloney SP, Pimiento JM, Fancher TT, Magri D, Westvik HH, Nishibe T, Velazquez OC, Dardik A. Limb ischemia after iliac ligation in aged mice stimulates angiogenesis without arteriogenesis. *J Vasc Surg*. 2009;49:464–473.

9. Rokutanda T, Izumiya Y, Miura M, Fukuda S, Shimada K, Izumi Y, Nakamura Y, Araki S, Hanatani S, Matsubara J, Nakamura T, Kataoka K, Yasuda O, Kaikita K, Sugiyama S, Kim-Mitsuyama S, Yoshikawa J, Fujita M, Yoshiyama M, Ogawa H. Passive exercise using whole-body periodic acceleration enhances blood supply to ischemic hindlimb. *Arterioscler Thromb Vasc Biol*. 2011;31:2872–2880.

10. Yu J, deMuinck ED, Zhuang Z, Drinane M, Kauser K, Rubanyi GM, Qian HS, Murata T, Escalante B, Sessa WC. Endothelial nitric oxide synthase is critical for ischemic remodeling, mural cell recruitment, and blood flow reserve. *Proc Natl Acad Sci U S A*. 2005;102:10999–11004.

11. Weyers JJ, Carlson DD, Murry CE, Schwartz SM, Mahoney WM Jr. Retrograde perfusion and filling of mouse coronary vasculature as preparation for micro computed tomography imaging. *J Vis Exp*. 2012;60:e3740.

12. Schindelin J, Arganda-Carreras I, Frise E, Kaynig V, Longair M, Pietzsch T, Preibisch S, Rueden C, Saalfeld S, Schmid B, Tinevez JY, White DJ, Hartenstein V, Eliceiri K, Tomancak P, Cardona A. Fiji: an open-source platform for biological-image analysis. *Nat Methods*. 2012;9:676–682.

13. Susaki EA, Tainaka K, Perrin D, Kishino F, Tawara T, Watanabe TM, Yokoyama C, Onoe H, Eguchi M, Yamaguchi S, Abe T, Kiyonari H, Shimizu Y, Miyawaki A, Yokota H, Ueda HR. Whole-brain imaging with single-cell resolution using chemical cocktails and computational analysis. *Cell*. 2014;157:726–739.

14. Arima Y, Miyagawa-Tomita S, Maeda K, Asai R, Seya D, Minoux M, Rijli FM, Nishiyama K, Kim KS, Uchijima Y, Ogawa H, Kurihara Y, Kurihara H. Preotic neural crest cells contribute to coronary artery smooth muscle involving endothelin signalling. *Nat Commun*. 2012;3:1267.

15. DeSesso JM. Vascular ontogeny within selected thoracoabdominal organs and the limbs. *Reprod Toxicol*. 2017;70:3–20.

16. Eshkar-Oren I, Viukov SV, Salameh S, Krief S, Oh CD, Akiyama H, Gerber HP, Ferrara N, Zelzer E. The forming limb skeleton serves as a signaling center for limb vasculature patterning via regulation of Vegf. *Development*. 2009;136:1263–1272.

17. Brantley SK, Rigdon EE, Raju S. Persistent sciatic artery: embryology, pathology, and treatment. *J Vasc Surg*. 1993;18:242–248.

18. Kawashima T, Sasaki H. Reasonable classical concepts in human lower limb anatomy from the viewpoint of the primitive persistent sciatic artery and twisting human lower limb. *Okajimas Folia Anat Jpn*. 2010; 87:141–149.

19. Ishizawa A, Hayashi S, Nasu H, Abe H, Rodriguez-Vazquez JF, Murakami G. An artery accompanying the sciatic nerve (arteria comitans nervi ischiadici) and the position of the hip joint: a comparative histological study using chick, mouse, and human foetal specimens. *Folia Morphol (Warsz)*. 2013;72:41–50.

20. Vaughan CL. Theories of bipedal walking: an odyssey. *J Biomech*. 2003;36:513–523.

21. Joosten SA, O'Driscoll DM, Berger PJ, Hamilton GS. Supine position related obstructive sleep apnea in adults: pathogenesis and treatment. *Sleep Med Rev*. 2014;18:7–17.

22. Guerin C, Reignier J, Richard JC, Beuret P, Gacouin A, Boulain T, Mercier E, Badet M, Mercat A, Baudin O, Clavel M, Chatellier D, Jaber S, Rosselli S, Mancebo J, Sirodot M, Hilbert G, Bengler C, Richecoeur J, Gainnier M, Bayle F, Bourdin G, Leray V, Girard R, Baboi L, Ayzac L; PROSEVA Study Group. Prone positioning in severe acute respiratory distress syndrome. *N Engl J Med*. 2013;368:2159–2168.

23. Charbord P. Bone marrow mesenchymal stem cells: historical overview and concepts. *Hum Gene Ther*. 2010;21:1045–1056.

24. Charbord P, Livne E, Gross G, Haupl T, Neves NM, Marie P, Bianco P, Jorgensen C. Human bone marrow mesenchymal stem cells: a systematic reappraisal via the genostem experience. *Stem Cell Rev*. 2011;7:32–42.

25. Dragneva G, Korpisalo P, Yla-Herttuala S. Promoting blood vessel growth in ischemic diseases: challenges in translating preclinical potential into clinical success. *Dis Model Mech*. 2013;6:312–322.